



UNIVERSITY OF LEEDS

This is a repository copy of *Design of Ge/SiGe quantum-confined Stark effect electroabsorption heterostructures for CMOS compatible photonics*.

White Rose Research Online URL for this paper:
<http://eprints.whiterose.ac.uk/42668/>

Article:

Lever, L, Ikonic, Z, Valavanis, A et al. (2 more authors) (2010) Design of Ge/SiGe quantum-confined Stark effect electroabsorption heterostructures for CMOS compatible photonics. *Journal of Lightwave Technology*, 28 (22). 3272 - 3281 (9). ISSN 0733-8724

<https://doi.org/10.1109/JLT.2010.2081345>

Reuse

See Attached

Takedown

If you consider content in White Rose Research Online to be in breach of UK law, please notify us by emailing eprints@whiterose.ac.uk including the URL of the record and the reason for the withdrawal request.



eprints@whiterose.ac.uk
<https://eprints.whiterose.ac.uk/>

Design of Ge–SiGe Quantum-Confined Stark Effect Electroabsorption Heterostructures for CMOS Compatible Photonics

Leon Lever, Zoran Ikonić, Alex Valavanis, Jonathan D. Cooper, and Robert W. Kelsall

Abstract—We describe a combined $6 \times 6 \mathbf{k} \cdot \mathbf{p}$ and one-band effective mass modelling tool to calculate absorption spectra in Ge–SiGe multiple quantum well (MQW) heterostructures. We find good agreement with experimentally measured absorption spectra of Ge–SiGe MQW structures described previously in the literature, proving its predictive capability, and the simulation tool is used for the analysis and design of electroabsorption modulators. We employ strain-engineering in Ge–SiGe MQW systems to design structures for modulation at 1310 nm and 1550 nm.

Index Terms—Modulation, quantum-confined Stark effect, quantum well devices.

I. INTRODUCTION

THE development of modulators that can be monolithically integrated with CMOS electronics is extremely desirable for applications including interconnects, high-speed networks and fiber-to-the-home (FTTH). Existing Mach–Zehnder modulators which exploit the plasma dispersion effect are large (several millimeters in length) and dissipate considerable amounts of power [1]. As such, there exists the requirement for compact low-power modulators that can be monolithically integrated with CMOS electronics [2].

The quantum-confined Stark effect (QCSE) is a shift in the absorption edge of a quantum-well heterostructure device under the application of an external electric field. Because of the reduced dimensionality of the system, the exciton binding energy is increased, and the excitonic peaks are preserved at room temperature [3], resulting in a higher achievable contrast in the absorption coefficient than is possible with the bulk Franz-Keldysh effect. The QCSE is an extremely rapid process, with intrinsic response times that are less than one pico-second [4]. Since the absorption coefficient of the multiple quantum well (MQW) material is large, the devices can be compact. Because of the compactness and the fact that no charge carrier accumulation or depletion is required, we can expect high bit-rates and low power consumption.

Manuscript received April 16, 2010; revised July 30, 2010, September 13, 2010; accepted September 16, 2010. Date of publication September 27, 2010; date of current version November 17, 2010. This work has been funded by the Engineering and Physical Sciences Research Council (EPSRC) program “U.K. Silicon Photonics.”

The authors are with the School of Electronic and Electrical Engineering, University of Leeds, Leeds LS2 9JT, U. K. (e-mail: l.j.m.lever@leeds.ac.uk; z.ikonic@leeds.ac.uk; a.valavanis@leeds.ac.uk; e106jdc@leeds.ac.uk; r.w.kelsall@leeds.ac.uk).

Color versions of one or more of the figures in this paper are available online at <http://ieeexplore.ieee.org>.

Digital Object Identifier 10.1109/JLT.2010.2081345

MQW electroabsorption modulators (EAMs) in III-V heterostructure systems can be monolithically integrated with semiconductor lasers and are widely used for optical-fibre telecommunications [5]–[8]. Ge–SiGe heterostructures can be epitaxially grown on Si substrates using reduced-pressure chemical vapour deposition (RP-CVD). Due to the lattice mismatch between Si and Ge it is necessary to grow the MQW stack on a relaxed SiGe *virtual substrate*. The QCSE in Ge–SiGe MQW systems was first observed in 2005 [9], where a contrast in the absorption coefficient of a factor of 4.69 was reported. The important wavelengths for telecommunications applications are 1310 nm and 1550 nm, and the operating wavelength for that device was ~ 1450 nm. Here we describe a simulation tool for calculating absorption spectra in Ge–SiGe MQW structures and report on device designs for EAMs where strain engineering is employed to target specific applications-oriented wavelengths (i.e., 1310 nm and 1550 nm). The paper is organized as follows. First, we describe the modelling technique used to calculate the bandstructure and absorption in the MQW active regions. Second, we compare our simulated data to experimentally measured data. Third, we describe the simulated absorption spectra of two devices—one designed to operate at 1310 nm and one at 1550 nm—and we examine the expected performance of waveguide-integrated devices based on these structures.

II. BANDSTRUCTURE

Optical absorption in Ge–SiGe MQW systems has been modelled previously using tight-binding [10], $\mathbf{k} \cdot \mathbf{p}$ [11], and tunnelling-resonance models [12]. The modelling method described here expands on these previous works, as we include interdiffusion of the Ge and SiGe layers, excitonic lineshapes based on the measured lifetimes of the electronic states, and the indirect absorption in the Ge quantum wells. A $6 \times 6 \mathbf{k} \cdot \mathbf{p}$ method [13] was used to calculate the valence bandstructure. The conduction band edge at Γ , L and Δ was determined using model-solid theory [14], [15], and the confined wavefunctions were calculated using a one-band effective mass model, which includes non-parabolicity of the conduction band.

Interdiffusion of the Ge and SiGe layers was accounted for by describing the Ge fraction as a function of position along the growth axis, $x(z)$, according to the following form [16]:

$$x(z) = \frac{1}{2} \sum_{I=1}^N \frac{x_I}{2} \left[\operatorname{erf} \left(\frac{z - z_{I-1}}{L_d} \right) - \operatorname{erf} \left(\frac{z - z_I}{L_d} \right) \right] + \frac{x_0}{2} \left[\operatorname{erf} \left(\frac{z - z_N}{L_d} \right) - \operatorname{erf} \left(\frac{z - z_0}{L_d} \right) \right] \quad (1)$$

where $\text{erf}()$ is the error function, I denotes the index of a given layer in the heterostructure, x_I is the nominal Ge fraction of that layer, x_0 is the Ge fraction at the start and end of the system, and L_d is a characteristic diffusion length.

To find the energies of the band edges, we first consider the unstrained case. The average energy of the light-hole (LH), heavy-hole (HH) and spin-orbit split-off (SO) valence band edges, relative to the average valence band edge in bulk Si (in electron volts), can be determined from [17]

$$\bar{E}_v = 0.55x. \quad (2)$$

This energy serves as a reference level, because it is strain invariant, and onto this we can add on terms for the bandgap, split-off energy, and energy shifts due to strain. In a strain-compensated Ge–SiGe MQW stack, because of the lattice mismatch, the Ge quantum wells will be compressively strained and the SiGe barriers will be tensile strained. Compressive strain splits the HH and LH bands such that the HH bands are higher in energy. Additionally, the confinement effective mass for the HH states is larger than the LH states. Consequently, we can expect the energy of the absorption edge to be determined by the energy of the HH quantized states. The HH band edge is given by

$$E_v^{\text{HH}} = \bar{E}_v + \frac{1}{3}\Delta_{\text{SO}} + \delta E_v^{\text{Hyd}} + \frac{1}{2}\delta E^{\text{Sh}} \quad (3)$$

where Δ_{SO} is the split-off energy, δE_v^{Hyd} is the shift in the valence band energy due to hydrostatic strain, given by

$$\delta E_v^{\text{Hyd}} = a_v(2\varepsilon_{\parallel} + \varepsilon_{\perp}) \quad (4)$$

where ε_{\parallel} is the in-plane strain, ε_{\perp} is the strain perpendicular to the growth plane, a_v is the valence band hydrostatic deformation potential, and δE^{Sh} is the shift in the valence band energy due to shear strain, given by

$$\delta E^{\text{Sh}} = 2b(\varepsilon_{\perp} - \varepsilon_{\parallel}) \quad (5)$$

where b is the valence band shear deformation potential.

The Γ -valley conduction band edge is located at

$$E_{\Gamma} = \bar{E}_v + \frac{1}{3}\Delta_{\text{SO}} - \delta E_c^{\text{Hyd}} + [E_{\Gamma_2}^{\text{Si}}(1-x) + E_{\Gamma}^{\text{Ge}}x - \delta_a x(1-x)] \quad (6)$$

where $E_{\Gamma_2}^{\text{Si}}$ is the Si Γ_2 bandgap, E_{Γ}^{Ge} is the Ge direct bandgap, $\delta_a = 0.23$ eV is the direct bandgap bowing parameter [18], and δE_c^{Hyd} is the shift in the conduction band energy due to hydrostatic strain, given by

$$\delta E_c^{\text{Hyd}} = a_c(2\varepsilon_{\parallel} + \varepsilon_{\perp}) \quad (7)$$

where a_c is the conduction band hydrostatic deformation potential.

The L - and Δ -valley conduction band edges were calculated similarly, and the relevant bandgap and deformation potential data is given in Table I, which summarizes the parameters used in the bandstructure calculation. The Δ -valley band edges are split so that there are four valleys with major axes in the

TABLE I
MATERIAL PARAMETERS USED IN THE BANDSTRUCTURE CALCULATIONS, INCLUDING THE LUTTINGER PARAMETERS USED IN THE $\mathbf{k} \cdot \mathbf{p}$ CALCULATION, γ_1 , γ_2 & γ_3 . NOTE THAT THE EFFECTIVE MASSES GIVEN HERE ARE THE QUANTIZATION EFFECTIVE MASSES, I.E., THOSE IN THE GROWTH DIRECTION, AND NOT TO BE CONFUSED WITH THE DENSITY OF STATES EFFECTIVE MASS USED IN SECTION III

Parameter	Si	Ge
γ_1	4.22 [20]	13.4 [20]
γ_2	0.39 [20]	4.25 [20]
γ_3	1.44 [20]	5.69 [20]
Δ_{SO} (eV)	0.044 [20]	0.296 [20]
a_{latt} (nm)	0.5431 [20]	0.5657 [20]
m_c^{Γ}	0.156 [21]	0.042 [22]
m_c^L	0.17 [23], [24]	0.12 [25]
$m_c^{\Delta_2}$	0.916 [26]	0.95 [26]
$m_c^{\Delta_4}$	0.19 [26]	0.2 [26]
E_{Γ} (eV)	4.0 [12]	0.8 [12]
E_L (eV)	2.01 [27]	0.66 [28]
E_{Δ} (eV)	1.11 [28]	0.931 [27]
a^{Γ} (eV)	-11.39 [29]	-8.97 [30]
a^L (eV)	-3.12 [14]	-2.78 [14]
a^{Δ} (eV)	1.72 [14]	1.31 [14]
a_v (eV)	2.46 [20]	1.24 [20]
a_c (eV)	$a + a_v$	$a + a_v$
b (eV)	-2.1 [31]	-1.88 [30]
b^{δ} (eV)	9.61 [14]	9.42 [14]

growth plane, and two valleys with the major axis in the growth direction.

The electron wavefunctions were calculated using a one-band effective mass approximation, where the conduction band effective mass in the heterostructure is determined according to

$$m_c(z) = x(z)m_c^{\text{Ge}} + [1 - x(z)]m_c^{\text{Si}} \quad (8)$$

and non-parabolicity was included using the method found in [19]. Linear interpolation was used to find the material parameters of the SiGe alloy layers, with the exception of the lattice constant, a_{latt} , where a bowing factor of 0.000188 nm was used [20].

III. OPTICAL ABSORPTION

We considered three contributions to the optical absorption—direct band-to-band transitions from valence subband states to Γ -valley subband states, which is evaluated at all in-plane wavevectors; indirect optical absorption, where valence electrons undergo a transition to a short-lived “virtual” Γ -valley conduction band state, and are scattered into a (much longer lifetime) L -valley state, which was also evaluated at all in-plane wavevectors; and excitonic contributions, where an electron–hole bound state is formed.

The band-to-band contribution to the absorption was calculated from [32]

$$\alpha_{\text{bb}}(\omega) = C_0 S_{2D} \frac{2}{L} \frac{1}{4\pi} \iint |\mathbf{e} \cdot \mathbf{p}|^2 dk_x dk_y \quad (9)$$

where L is the periodicity of the MQW system (i.e., the well width plus the barrier width), $|\mathbf{e} \cdot \mathbf{p}|$ is the momentum matrix element between the electron and hole wavefunctions, k_x and

k_y are the wave vectors in the growth plane, the factor of two accounts for spin degeneracy, and C_0 is given by

$$C_0 = \frac{\pi e^2}{N_r c \epsilon_0 m_0^2 \omega} \quad (10)$$

where ω is the angular frequency of the light and N_r is the real part of the refractive index of the material, where a linear interpolation between Si and Ge was used to describe the refractive index of a material with the average composition of the MQW system. S_{2D} is the Coulomb enhancement factor, which is given by [33]

$$S_{2D} = \frac{e^{\pi/\sqrt{\Delta}}}{\cosh(\pi/\sqrt{\Delta})} \quad (11)$$

where Δ is the total excess kinetic energy of the electron-hole pair normalized to $E_b/4$, where E_b is the exciton binding energy. Since there is no straight-forward dispersion relation for holes, the excess kinetic energy of electrons only was used. This is justified because the effective mass of the Γ -valley electrons is much smaller than that for holes.

The absorption calculation was implemented as a numerical integration over finite in-plane wavevectors. For each finite region of k -space and for each pair of subbands, a Gaussian-broadened contribution to the spectra was found, and these were summed to generate the resultant spectra. This Gaussian broadening both facilitates the numerical calculation and allows us to incorporate the inhomogeneous broadening that occurs due to fluctuations in the dimensions of the quantum wells throughout the structure. There is no literature value for this, and so it is effectively a fitting parameter. We used a half-width-at-half-maximum (HWHM) of 5 meV, which was chosen to match the experimental data discussed in Section IV.

Indirect absorption was included based on the method described in [34], and is given by

$$\begin{aligned} \alpha_{\text{in}}(\omega) = & C_0 S_{2D} \frac{2}{L} \frac{1}{4\pi} \frac{\hbar D_q^2 N_{\text{val}}}{2\rho\omega_q} \\ & \times \int \int |\mathbf{e} \cdot \mathbf{p}|^2 \frac{1}{(E_0 - \hbar\omega)^2} [N\rho_L(E_k^L + \hbar\omega_q) \\ & + (N+1)\rho_L(E_k^L - \hbar\omega_q)] dk_x dk_y, \end{aligned} \quad (12)$$

where $D_q = 4.2 \times 10^8$ eV/cm is the deformation potential for $\Gamma \rightarrow L$ scattering [35], $N_{\text{val}} = 4$ is the number of destination valleys, $\omega_q = 28$ meV/ \hbar is the phonon angular frequency [35], ρ is the mass density, N is the Bose-Einstein factor for the intervalley phonon, ρ_L is the density of states in the L -valley and E_k^L is the kinetic energy of the L -valley final state. The term E_0 is the energy of the direct optical transition, and must be modified from the bulk case according to

$$E_0 = E_\Gamma + E_e + E_h \quad (13)$$

where E_Γ is the Ge Γ bandgap (which here accounts for the effects of strain), and E_e and E_h are k -space dependent electron and hole state energies for a given Γ -valley subband (i.e., the confinement energy of the subband minima plus the kinetic energy). Note that the value of S_{2D} will differ from that in (9)

because the kinetic energy of the electron-hole pair is that of an L -valley electron and because the exciton binding energy is larger because of the larger effective mass of the L -valley electrons.

The L -valley conduction band edge is approximately 140 meV lower in energy than the Γ -valley. In the range of photon energies close to the absorption edge we can expect that there will be multiple subbands available in the indirect absorption process. Therefore, the density of states in the destination L -valley will be well approximated by a bulk description, and ρ_L was calculated assuming a three-dimensional parabolic dispersion relation and using an effective mass of 0.22 m_0 [36].

When the photon energy approaches E_0 , the perturbation theory upon which (12) is based breaks down. Therefore, for the range of photon energies where the direct contribution to the absorption exceeds the indirect contribution, we consider only the former.

The excitonic contributions to the spectra were found using a variational energy minimization approach [37], [38]. The exciton wavefunction was assumed to be of the form

$$\phi(r) = \sqrt{\frac{2}{\pi}} \frac{1}{\lambda} e^{-r/\lambda} \quad (14)$$

where r is a parameter describing the separation of the electron and hole wavefunctions, and λ is the variational parameter (which can be thought of as the Bohr radius of the exciton).

In III-V quantum well systems, the lifetime of the Γ -valley states is greater than 1 ps, and so the lifetime broadening is much less than 1 meV and the dominant contribution to the linewidths for optical transitions is due to structural disorder. Consequently, the exciton lineshapes can be described by a Gaussian [39]. In Ge-SiGe systems however, there is rapid $\Gamma \rightarrow L$ scattering, and the lifetime of the Γ -valley confined states is much shorter, which means that the lifetime broadening of the excitons becomes significant. We do not consider lifetime broadening of the direct band-to-band optical absorption term α_{bb} because this effect is accounted for in the indirect absorption. However, virtual excitonic states do not feature in the calculation of α_{in} , and so we include a homogeneous broadening component in the exciton lineshapes.

Excitonic lineshapes were modelled according to the Voigt profile, and we included a lifetime (Lorentzian) broadening HWHM of $\Gamma_L = 3$ meV, which corresponds to a Γ -valley conduction band lifetime of 110 fs [40], and an inhomogeneous (Gaussian) HWHM of $\gamma = 5$ meV. The resulting excitonic contribution to the absorption spectrum due to each pair of electron and hole subbands is then given by

$$\alpha_{\text{ex}} = \frac{2C_0}{L} |\mathbf{e} \cdot \mathbf{p}|^2 \frac{2}{\pi\lambda^2} V(E_{i,j} - E_b, \hbar\omega, \Gamma_L, \gamma) \quad (15)$$

where $E_{i,j}$ is the energy difference between a given pair of subband minima, E_b is the exciton binding energy, and $V()$ is the Voigt profile, which was modelled numerically using the method found in [41].

IV. RESULTS

We compared our simulated data to the experimental data in [9]. The MQW section of that device consisted of 10-nm-thick Ge quantum wells and 16-nm-thick $\text{Si}_{0.15}\text{Ge}_{0.85}$ barriers, and

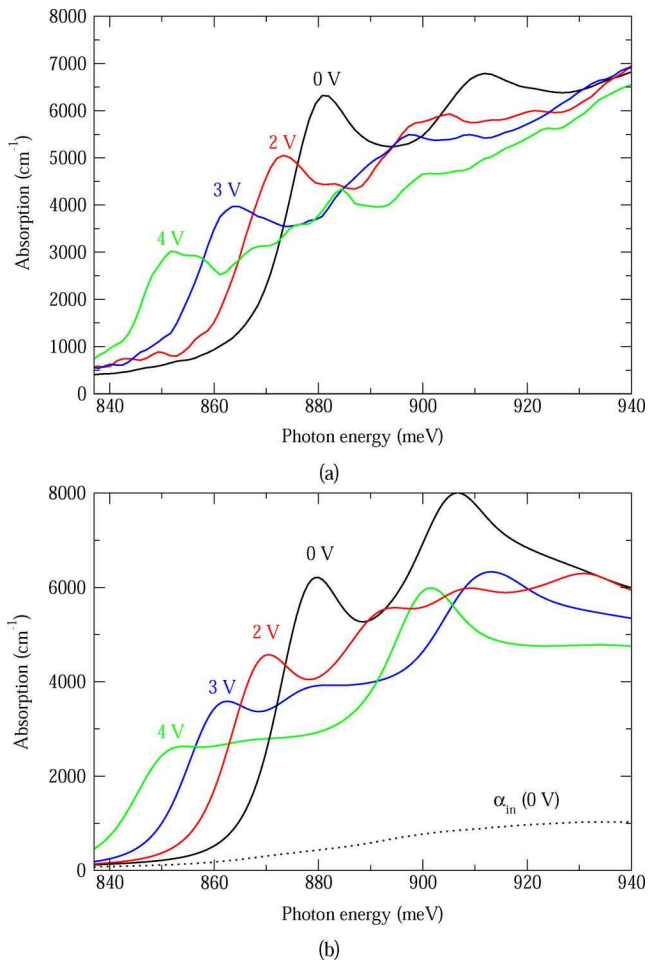


Fig. 1. (a) Experimental absorption spectra using the data from Kuo *et al.* [9]; (b) simulated absorption spectra, with the indirect absorption at 0 V shown by the dotted line. The electric fields used in the simulation were determined by considering the built-in p - n junction bias of 800 meV plus the applied bias, which is dropped across the width of the intrinsic region minus 75 nm to account for diffusion of dopants [42]. Both spectra are for TE-polarized light.

was grown on a $\text{Si}_{0.1}\text{Ge}_{0.9}$ virtual substrate. A comparison between the measured absorption spectra and our simulated data is shown in Fig. 1 at a range of applied biases. We find very satisfactory agreement in the position of the excitonic peaks and the observed Stark shift.

Recent studies [43], [44] have shown that CVD grown Ge thin films on Si substrates are tensile strained. This residual tensile strain arises because the bulk thermal expansion coefficient of Ge is larger than that of the Si substrate, and as the structure cools from the growth temperature the Ge epilayer is constrained to shrink by the amount that the substrate shrinks. Ge that is grown on an Si substrate by CVD (and allowed to cool to room temperature) typically experiences a tensile strain of 0.15%–0.2%, which results in bandgap shrinkage of 20–30 meV [43]–[46]. Ishikawa *et al.* showed that the residual tensile strain in Ge thin films increases approximately proportionally with the growth/annealing temperature and saturates at 750°C. The 0.15–0.2% tensile strain value given above corresponds to samples that were grown/annealed above 750°C, however, the virtual substrates (and we can expect the MQW region to be lattice-matched to the virtual substrate) in [9] were grown and an-

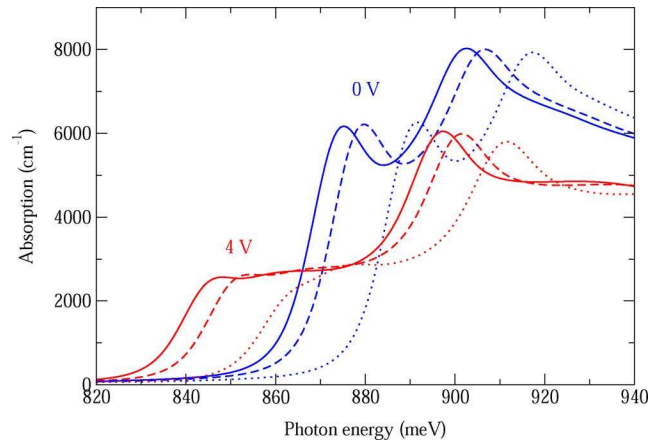


Fig. 2. Absorption spectra at 0 V and 4 V for different values of the interdiffusion length. The solid curves are for $L_d = 0$, the dashed for $L_d = 1$ nm and the dotted for $L_d = 2$ nm.

nealed at 700°C. Additionally, the virtual substrates were composed of $\text{Si}_{0.1}\text{Ge}_{0.9}$. These two considerations mean that we may expect approximately 80% of the bandgap shrinkage that was observed in the samples in [43]–[46] (i.e., 0.12–0.16% tensile strain). We find agreement with the position of the absorption edge if a residual tensile strain of 0.1% is included, which is in reasonable agreement with the analysis just presented.¹

Fig. 2 shows the simulated absorption spectra as a function of the interdiffusion length, L_d . As L_d is increased, we see an increasing blue-shift of the absorption edge. Interdiffusion has a larger effect on the energy of the confined electron wavefunctions than energy of the hole wavefunctions because the effective mass of electrons is much smaller. Since the confined electron states have energies near the bottom of the well, we can think of increasing L_d as making the the well narrower, hence increasing the energy of the subband minimum. Note that it is possible to achieve agreement with the position of the absorption edge (i.e., the $hh_1 \rightarrow e_1$ exciton) using 0.15%–0.2% residual tensile strain together with a larger value of L_d . However, this would result in less compressive strain in the Ge quantum wells and so a smaller LH/HH splitting, and we would lose agreement with the energy of the $lh_1 \rightarrow e_1$ exciton. We have chosen $L_d = 1$ nm and 0.1% tensile strain to best reproduce the experimental data.

The calculated sub-band-gap absorption coefficient is approximately a factor of three smaller than the data in [9], which shows a significant low-energy tail to the absorption spectra. This was attributed to indirect absorption, however, as is clear from Fig. 1 our calculated indirect contribution to absorption is weaker than the total measured sub-band-gap absorption coefficient. A possible explanation for the discrepancy is absorption due to lattice defects. Highly-strained heteroepitaxial samples of III-V compounds on Si substrates have large threading dislocation densities (TDDs), and this results in considerable sub-band-gap absorption (for example, GaAs with a TDD of $3 \times 10^9 \text{ cm}^{-2}$ had a sub-band-gap absorption coefficient of around 5000 cm^{-1}) [47]. SiGe virtual

¹Furthermore, the virtual substrate used by Kuo *et al.* was doped, and so this may have some additional effect on the residual tensile strain *c.f.* the undoped samples in [43]–[46].

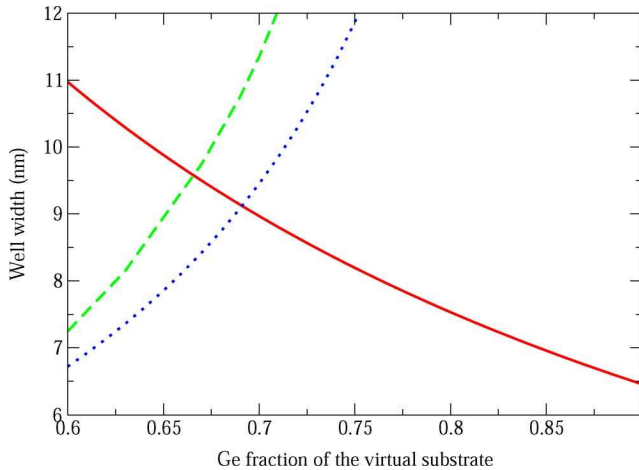


Fig. 3. Solid line shows the combination of substrate composition and well thickness required to achieve a detuning of the absorption edge of 25 meV in a Ge-Si_{0.4}Ge_{0.6} quantum well. The dotted line shows the critical thickness calculated according to Van der Merwe and the dashed line according to Matthews and Blakeslee using the expressions given in [50]. A residual tensile strain of 0.1% was assumed.

substrates such as were used for the epitaxial growth of the samples in [9] have threading dislocation densities of the order of 1×10^7 to $1 \times 10^8 \text{ cm}^{-2}$ [48], and so this defect population may account for the additional component of the sub-band-gap absorption. Absorption spectra in similar Ge-SiGe quantum well structures employing thick graded buffers [40] show a sub-band-gap component that is smaller than that in [9], and in better agreement with the modelling results described here. Hence, there may be scope for optimizing the sub-band-gap absorption, and TDDs may be an important factor in this. Any reduction of sub-band-gap absorption is significant because it improves both the insertion loss and extinction ratio of an EAM device.

V. MQW DESIGN USING STRAIN ENGINEERING

Many fiber-optic telecommunications systems exploit the spectral ‘window’ at 1310 nm, which corresponds to zero dispersion in standard single-mode optical fibers. Passive optical network architectures typically use 1310 nm for upstream signals [49], and so compact, low-cost and low-power modulators operating at 1310 nm that can be integrated into Si electronic-photonic integrated circuits would be extremely desirable for emerging FTTH applications.

1310-nm light corresponds to a photon energy of 946 meV. This requires a considerable blue-shift of the absorption edge compared to that of bulk Ge, so that the system can be transparent in the on state (i.e., transmitting, with a low or zero electric field). This can be achieved by using extremely narrow quantum wells; however, it would require a very large electric field to produce a significant Stark shift. Alternatively, using SiGe quantum wells would result in an increase of the direct bandgap; however, very precise control over the Si content would be required. The third option is to use strain engineering.

Compressive strain results in an increase of the Ge direct band-gap, and the Ge layers will experience larger compressive strain as the Si content of the virtual substrate is increased. The growth of the Ge epilayer on the SiGe virtual substrate results in

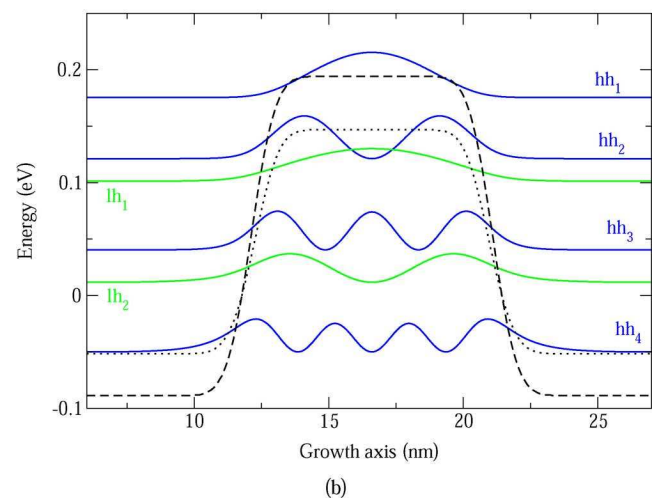
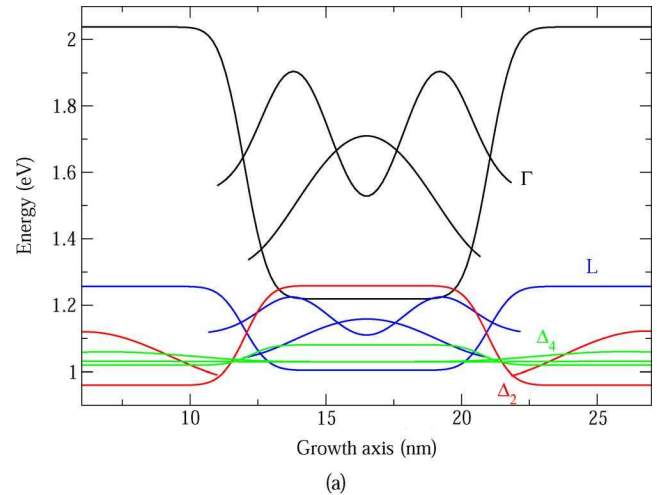


Fig. 4. (a) Zero-field conduction band edges at Γ , L and Δ , together with the two lowest lying electron wavefunctions in each valley. The Δ -valleys are split due to strain, with the two valleys with their major axes in the growth direction (Δ_2) having a larger band offset than the four valleys with their major axes in the growth plane (Δ_4). (b) Valence bandstructure; the HH band edge is shown by the dashed line and the LH band edge by the dotted line.

the accumulation of energy in the strained layer, and each layer must not exceed the critical thickness, h_c , beyond which it becomes energetically favourable for the strain to relax via dislocations in the crystal structure. Fig. 3 shows the combination of substrate composition and well dimensions required to achieve a detuning of the absorption edge of 25 meV from 946 meV (i.e., to increase the zero-field absorption to 971 meV). Also shown is h_c calculated according to two methods described in [50]. The electric field required to achieve a given Stark shift is larger for narrower quantum wells, hence it is preferable to use wider quantum wells. However, to ensure h_c is not exceeded, we are constrained to choosing combinations of material parameters that lie on the right-hand side of the dotted line in Fig. 3.

Our design uses a Si_{0.3}Ge_{0.7} virtual substrate with 9-nm-wide Ge QWs and Si_{0.4}Ge_{0.6} barriers, and strain-compensation [13] requires that the barriers are 12-nm-wide. Fig. 4 shows the bandstructure for the MQW system. In the valence band there is considerable splitting of the HH and LH states, and in the conduction band we can see that the quantum wells are type-I in both L and Γ , and are type-II at the Δ points. Fig. 5 shows

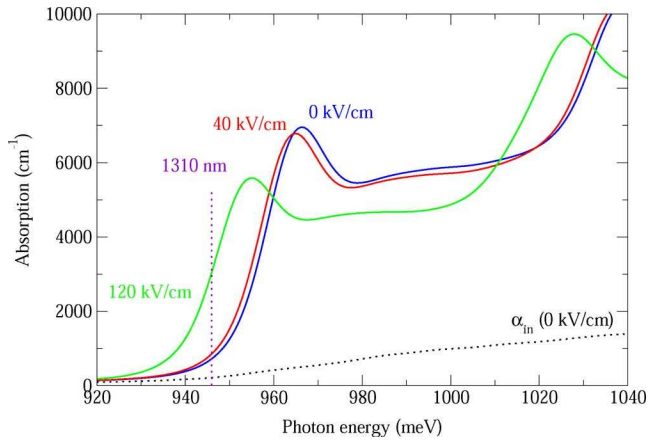


Fig. 5. TE-polarized absorption spectra of the 9-nm-wide $\text{GeSi}_{0.4}\text{Ge}_{0.6}$ MQW structure at various applied fields. At zero field a simulated absorption coefficient at 1310 nm of 720 cm^{-1} is observed, and we find this increases to 840 cm^{-1} under an applied field of 40 kV/cm, and to 3060 cm^{-1} under an applied field of 120 kV/cm.

the simulated absorption spectra for the MQW system. The increased strain-splitting of the HH and LH states can be seen in the spectra, and only $hh_1 \rightarrow e_1$ is significant near to the absorption edge. A difference in the simulated absorption coefficient at 1310 nm of 2220 cm^{-1} is observed between applied fields of 40 kV/cm and 120 kV/cm.

The Γ -valley conduction band offset at the $\text{GeSi}_{0.4}\text{Ge}_{0.6}$ interface is large, almost 800 meV. This may be expected to lead to difficulties in extracting electrons, limited by thermionic emission over the barriers. However, as has already been discussed, the Γ valley electrons are rapidly scattered to lower-lying X and (in particular) L valleys, and as we can see from Fig. 4, these are much more weakly bound even with the relatively large Si fraction in the barriers, and therefore we can expect no such problems with extraction of electrons.

1550 nm corresponds to the minimum loss in standard single-mode optical fibres, and so is an attractive wavelength for telecommunications applications. The direct bandgap of Ge changes with temperature, and EA modulation at 1550 nm has been achieved using an elevated temperature of 100°C in an MQW system with 15-nm-thick Ge quantum wells and $\text{Si}_{0.16}\text{Ge}_{0.84}$ barriers on a $\text{Si}_{0.1}\text{Ge}_{0.9}$ virtual substrate [51].

A system with less compressive strain in the Ge quantum wells was demonstrated at an elevated temperature of 90°C , with 12.5-nm-wide Ge QWs, $\text{Si}_{0.175}\text{Ge}_{0.825}$ barriers, and a $\text{Si}_{0.05}\text{Ge}_{0.95}$ virtual substrate [52]. The room-temperature absorption edge of that device was 1456 nm (which is in excellent agreement with our simulated value of 1455 nm) and shifted to 1508 nm when the temperature was increased to 90°C . By increasing the width of the quantum wells to 16 nm we find that the simulated room-temperature zero-field absorption edge shifts to 1490 nm and that EA modulation is expected at 1550 nm, which is consistent with the analysis presented in [11]. However, we also find that the simulated absorption coefficient at 1550 nm with an applied electric of 80 kV/cm falls to only 1100 cm^{-1} . This means that a long device would be required to achieve absorption in the off state and, given the additional losses in the system, means that poor performance

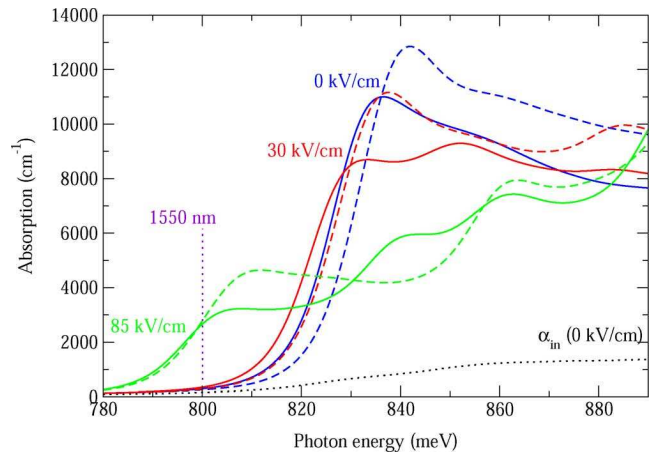


Fig. 6. Absorption spectra of the 14-nm-wide MQW structure at applied fields of 0 kV/cm, 30 kV/cm and 85 kV/cm. The TE-polarized spectra are shown as solid lines and the TM-polarized spectra as dashed lines. At zero field a simulated absorption coefficient at 1550 nm of 280 cm^{-1} is observed, and at 30 kV/cm it is 320 cm^{-1} . We find this increases to 2740 cm^{-1} under an applied field of 85 kV/cm for both TE- and TM-polarized light. Because of the reduced compressive strain in the Ge quantum wells, the light- and heavy-hole excitons are so close in energy that they cannot be resolved in the TE spectra, and a single peak in the zero-field absorption spectrum is seen at 835 meV. The TM spectra does not contain a peak for the heavy-hole exciton, and so the absorption edge is slightly blue shifted with respect to the TE spectra. The indirect contribution to the absorption at zero field is shown for TE only as there is little difference between the TE- and TM-polarized indirect absorption.

would be expected. This is because the wider quantum wells result in larger spatial separation of the electron and hole wavefunctions when the electric field is applied.

Narrower wells can be used to improve the contrast in the absorption coefficient between the on and off states. To target 1550-nm light an increase in the Ge fraction of the substrate is required. Fig. 6 shows absorption spectra for 14-nm-wide Ge quantum wells with 6-nm-wide $\text{Si}_{0.15}\text{Ge}_{0.85}$ barriers on a $\text{Si}_{0.025}\text{Ge}_{0.975}$ virtual substrate. The increased Ge fraction of the virtual substrate reduces the strain-splitting of the heavy-hole and light-holes states. This results polarization-independent operation at 1550 nm, and we find a difference in the absorption coefficient of approximately 2420 cm^{-1} in both polarizations.

When using such a high Ge fraction in the virtual substrate there are two design challenges that must be carefully considered. First, the absorption edge of the virtual substrate itself becomes close to the carrier wavelength. We can determine the direct bandgap of the (relaxed) $\text{Si}_{0.025}\text{Ge}_{0.975}$ virtual substrate from the term in square brackets in (7), which gives 863 meV, and is considerably larger than the photon energy. The data in [53] suggests that the $\text{Si}_{0.025}\text{Ge}_{0.975}$ virtual substrate will have losses of approximately 60 cm^{-1} at 1550 nm. Second, strain compensation requires that the $\text{Si}_{0.15}\text{Ge}_{0.85}$ barriers are 2-nm-thick. Such thin barriers will result in hybridization of the wavefunctions belonging to adjacent quantum wells, and the interaction energy will lead to a broadening of the absorption edge. Such behaviour is not desirable, and it is preferable to use thicker barriers to isolate the wavefunctions belonging to adjacent quantum wells. We performed tunnelling linewidth calculations [54] using a scattering matrix method [55] within the $\mathbf{k} \cdot \mathbf{p}$ framework employed here to determine the additional broadening. Fig. 7 shows the tunnelling linewidths as a function

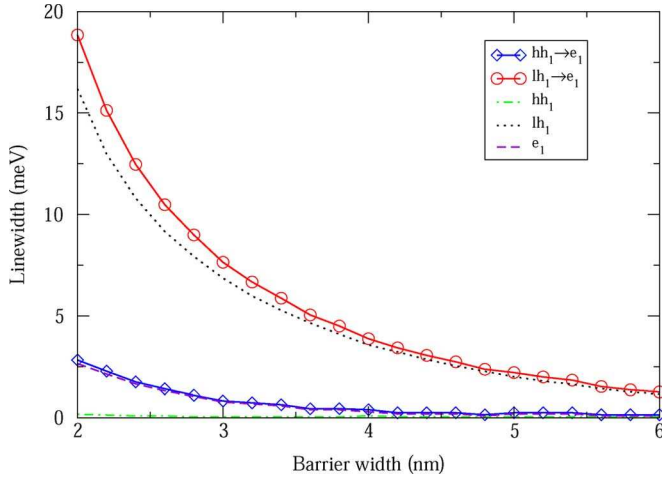


Fig. 7. Tunnelling FWHM linewidths of the hh_1 , lh_1 and e_1 states in a $\text{Si}_{0.15}\text{Ge}_{0.85}$ double-barrier structure surrounding a 14-nm Ge quantum well on a $\text{Si}_{0.025}\text{Ge}_{0.975}$ virtual substrate.

of the barrier width for the 14-nm quantum wells. These additional linewidths were added to the Gaussian component of the exciton linewidths to calculate the absorption spectra shown in Fig. 6, where 6-nm-thick barriers were used.

The Matthews-Blakeslee formula gives a critical thickness of 16 nm for the $\text{Si}_{0.15}\text{Ge}_{0.85}$ barriers. Although this is not exceeded by a single 6-nm-thick barrier, an MQW stack containing ten quantum wells and eleven barriers would accumulate almost three times more strain energy than a single h_c -thick layer. On high-purity substrates, the Matthews-Blakeslee critical thickness can be exceeded, and a metastable regime is formed where relaxation is inhibited by the kinetic barrier to defect formation; however, this is not the case for SiGe virtual substrates because of the large defect density [50]. More importantly, in multi-layered compressive/tensile strained structures, the metastable limit is extended [56], and accumulated strain in compressive/tensile structures has been reported equivalent to six times the (metastable) critical thickness [57]. Consequently, we can expect that the structures we propose will be mechanically stable.

VI. EXPECTED DEVICE PERFORMANCE

To evaluate the performance of these structures for use in waveguide-integrated EAMs, we calculated the fundamental modes in a cross section of a device using finite element method (FEM) modelling [58]. A mesa-etched device was modelled, with a 400-nm-thick p -type Si substrate with a doping level of $5 \times 10^{18} \text{ cm}^{-3}$, a 500-nm-thick p -type virtual substrate with a doping level of $5 \times 10^{18} \text{ cm}^{-3}$, a 50-nm-thick intrinsic spacer layer, the MQW stack, a second 50-nm-thick spacer layer, a 100-nm-thick n -type Ge layer with a doping level of $1 \times 10^{19} \text{ cm}^{-3}$, and a top contact layer. The spacer layers are included to maintain a constant electric field across the whole of the MQW stack, and we have modelled ten quantum wells and eleven barriers giving a ~ 200 -nm-thick active region. No coupling loss to the incoming and outgoing Si waveguides was considered, and it was assumed that the incoming waveguide excites only the fundamental mode of the structure.

TABLE II

LOSSES IN cm^{-1} FOR EACH LAYER OF THE WAVEGUIDE-INTEGRATED DEVICE. $\alpha_{\text{interband}}$ IS THE INTERBAND LOSS, WHICH IN THE SiGe VIRTUAL SUBSTRATE LAYERS IS INDIRECT ABSORPTION USING THE DATA FROM [53], AND IN THE MQW LAYERS IS THE SIMULATED ABSORPTION IN THE ON AND OFF STATES. α_{fcl} IS THE FREE CARRIER LOSSES IN THE DOPED LAYERS

Layer	1310 nm		1550 nm	
	α_{fcl}	$\alpha_{\text{interband}}$	α_{fcl}	$\alpha_{\text{interband}}$
p -Si	15.8	-	22.4	-
p -SiGe VS	4.5	20	6.4	60
i -SiGe VS	-	20	-	60
n -SiGe VS	15.2	20	21.7	60
MQW _{On}	-	840	-	320
MQW _{Off}	-	3060	-	2740

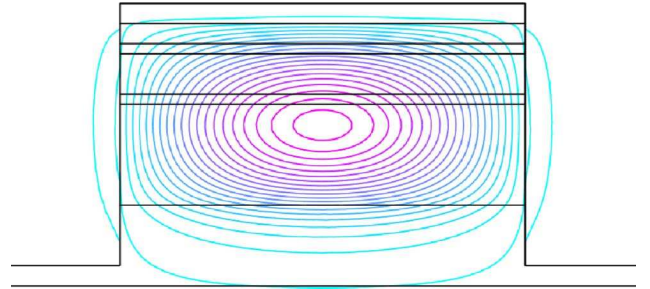


Fig. 8. Waveguide device structure with the fundamental TE mode at 1310 nm shown as a contour plot. The layer structure is (from the bottom) p -Si, p -SiGe, i -SiGe, MQW, i -SiGe, n -SiGe, Cu, and the cladding is SiO_2 .

The losses in each semiconductor layer are listed in Table II. Free-carrier losses were found using the Drude model [13], the band-to-band absorption of the virtual substrate was estimated using the data in [53], and the MQW absorption coefficients were taken from the simulated data in the previous section. While the best performance can be achieved by considering the difference between the zero-field absorption, to reduce the peak-to-peak drive bias we chose to use the absorption at 40 kV/cm for the 1310 nm device and 30 kV/cm for the 1550 nm device.

The fundamental TE mode profile in the waveguide device is shown in Fig. 8 at 1310 nm. The losses in the Cu top contact were taken as $860\,000 \text{ cm}^{-1}$ [59]. We find total waveguide losses for the 2- μm -wide etched structure of 200 cm^{-1} in the on state and of 645 cm^{-1} in the off state. For a 40- μm -long device, this corresponds to an extinction ratio of 7.7 dB and an insertion loss of 3.5 dB.

In order to obtain polarization independence at 1550 nm, the Cu top contact layer in the device was replaced with a doped polysilicon top contact, because the metal layer results in a significant difference between the mode profiles of the two polarizations. We assumed losses of 5000 cm^{-1} in the polysilicon layer. The mode profile is shown in Fig. 9. We find waveguide losses of 155 cm^{-1} in the on state and of approximately 740 cm^{-1} in the off state for both TE and TM polarizations. For a 40- μm -long device, this corresponds to an extinction ratio of approximately 10.2 dB and an insertion loss of 2.7 dB in both polarizations.

The response time of these EAM devices can be estimated by treating them as parallel-plate capacitors. The 80- μm^2 mesa

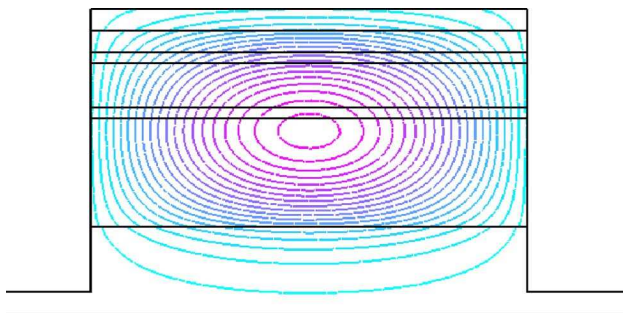


Fig. 9. Waveguide device structure with the fundamental TE mode at 1550 nm shown as a contour plot. The geometry of the structure means that the TM mode profile is very similar, and so this is not shown. The layer structure is (from the bottom) p -Si, p -SiGe, i -SiGe, MQW, i -SiGe, n -SiGe, n -polysilicon, and the cladding is SiO₂.

devices with a 300-nm-thick intrinsic region will have a capacitance of approximately $C = 35$ fF. If we assume a 50- Ω load resistance, this will result in a time constant $RC = 1.8$ ps, making the devices suitable for operation at 40 Gb/s.

The devices will dissipate power both due to the photo-generated charge carrier pairs, and to losses associated with the capacitance. For high bit-rate EAM applications the photocurrent results in losses that are small compared to the capacitive losses [60]. The energy per bit can therefore be estimated from $1/2CV_{pp}^2$, where V_{pp} is the peak-to-peak drive voltage. For the 1310 nm device, $V_{pp} = 2.4$ V, and so we can expect the power consumption to be approximately 100 fJ/bit. For the 1550 nm device, $V_{pp} = 1.65$ V, and so we can expect the power consumption to be approximately 50 fJ/bit.

VII. CONCLUSION

We have described a combined 6×6 $k \cdot p$ and one-band effective mass model to calculate the absorption spectra of Ge–SiGe MQW heterostructures. Using the simulation tools, Ge–SiGe quantum well structures on SiGe virtual substrates were identified to target the spectral windows at 1310 nm and 1550 nm by exploiting the strain due to epitaxial growth on the SiGe virtual substrate. The expected performance of waveguide-integrated devices based on these MQW heterostructures was analysed, and we can expect small footprint devices ($< 100\text{-}\mu\text{m}^2$ device area) with a power consumption of the order of 100 fJ/bit and capable of operation at data rates of 40 Gb/s.

REFERENCES

- [1] L. Liao, A. Liu, D. Rubin, J. Basak, Y. Chetrit, H. Nguyen, R. Cohen, N. Izhaky, and M. Paniccia, "40 gbit/s silicon optical modulator for high-speed applications," *Electron. Lett.*, vol. 43, 2007.
- [2] D. Miller, "Device requirements for optical interconnects to silicon chips," *Proc. IEEE*, vol. 97, no. 7, pp. 1166–1185, Jul. 2009.
- [3] D. A. B. Miller, D. S. Chemla, T. C. Damen, A. C. Gossard, W. Wiegmann, T. H. Wood, and C. A. Burrus, "Band-edge electroabsorption in quantum well structures: The quantum-confined Stark effect," *Phys. Rev. Lett.*, vol. 53, no. 22, pp. 2173–2176, Nov. 1984.
- [4] S. Schmitt-Rink, D. S. Chemla, W. H. Knox, and D. A. B. Miller, "How fast is excitonic electroabsorption?," *Opt. Lett.*, vol. 15, no. 1, pp. 60–62, 1990.
- [5] T. H. Wood, "Multiple quantum well (MQW) waveguide modulators," *J. Lightw. Technol.*, vol. 6, no. 6, pp. 743–757, Jun. 1998.
- [6] T. Ido, S. Tanaka, M. Suzuki, and H. Inoue, "MQW electroabsorption optical modulator for 40 Gbit/s modulation," *Electron. Lett.*, vol. 31, no. 24, pp. 2124–2125, 1995.
- [7] A. Ramdane, F. Devaux, N. Souli, D. Delprat, and A. Ougazzaden, "Monolithic integration of multiple-quantum-well lasers and modulators for high-speed transmission," *IEEE J. Sel. Top. Quantum Electron.*, vol. 2, no. 2, pp. 326–335, Mar./Apr. 1996.
- [8] R. Lewén, S. Irmscher, U. Westergren, L. Thylén, and U. Eriksson, "Segmented transmission-line electroabsorption modulators," *J. Lightw. Technol.*, vol. 22, no. 1, pp. 172–179, Jan. 2004.
- [9] Y.-H. Kuo, Y. K. Lee, Y. Ge, S. Ren, J. E. Roth, T. I. Kamins, D. A. B. Miller, and J. S. Harris, "Strong quantum-confined Stark effect in germanium quantum-well structures on silicon," *Nature*, vol. 437, pp. 1334–1336, 2005.
- [10] M. Virgilio and G. Grosso, "Quantum-confined stark effect in Ge–SiGe quantum wells: A tight-binding description," *Phys. Rev. B*, vol. 77, no. 16, p. 165315, 2008.
- [11] D. J. Paul, "8-band $k \cdot p$ modeling of the quantum confined stark effect in Ge quantum wells on Si substrates," *Phys. Rev. B*, vol. 77, no. 15, p. 155323, 2008.
- [12] R. K. Schaevitz, J. E. Roth, S. Ren, O. Fidaner, and D. A. Miller, "Material properties of Si-Ge–Ge quantum wells," *IEEE J. Sel. Topics Quantum Electron.*, vol. 14, no. 4, pp. 1082–1089, Jul./Aug. 2008.
- [13] P. Harrison, *Quantum Wells, Wires and Dots: Theoretical and Computational Physics of Semiconductor Nanostructures*, 3rd ed. Chichester, U.K.: Wiley, 2009.
- [14] C. G. Van de Walle and R. M. Martin, "Theoretical calculations of heterojunction discontinuities in the Si/Ge system," *Phys. Rev. B*, vol. 34, no. 8, pp. 5621–5634, 1986.
- [15] C. G. Van de Walle, "Band lineups and deformation potentials in the model-solid theory," *Phys. Rev. B*, vol. 39, no. 3, pp. 1871–1883, Jan. 1989.
- [16] E. Li, B. Weiss, and K.-S. Chan, "Eigenstates and absorption spectra of interdiffused AlGaAs–GaAs multiple-quantum-well structures," *IEEE J. Quantum Electron.*, vol. 32, no. 8, pp. 1399–1416, Aug. 1996.
- [17] V. V. Afanas'ev, A. Stesmans, L. Souriau, R. Loo, and M. Meuris, "Valence band energy in confined Si_{1-x}Ge_x (0.28 < x < 0.93) layers," *Appl. Phys. Lett.*, vol. 94, no. 17, p. 172106, 2009.
- [18] F. Tekia, M. Ferhat, and A. Zaoui, "Band-gap bowing in Si_xGe_{1-x} alloy," *Phys. B: Cond. Matt.*, vol. 293, no. 1–2, pp. 183–186, 2000.
- [19] D. F. Nelson, R. C. Miller, and D. A. Kleinman, "Band nonparabolicity effects in semiconductor quantum wells," *Phys. Rev. B*, vol. 35, no. 14, pp. 7770–7773, May 1987.
- [20] M. Kahan, M. Chi, and L. Friedman, "Infrared transitions in strained-layer Ge_xSi_{1-x}/Si," *J. Appl. Phys.*, vol. 75, pp. 8012–8021, 1994.
- [21] M. Fischetti, "Monte Carlo simulation of transport in technologically significant semiconductors of the diamond and zinc-blende structures. I. Homogeneous transport," *IEEE Trans. Electron. Devices*, vol. 38, no. 3, pp. 634–649, Mar. 1991.
- [22] M. Cardona and F. H. Pollak, "Energy-band structure of germanium and silicon: The $k \cdot p$ method," *Phys. Rev.*, vol. 142, no. 2, pp. 530–543, 1966.
- [23] M. M. Rieger and P. Vogl, "Electronic-band parameters in strained Si_{1-x}Ge_x alloys on Si_{1-y}Ge_y substrates," *Phys. Rev. B*, vol. 48, no. 19, pp. 14 276–14 287, 1993.
- [24] M. V. Fischetti and S. E. Laux, "Band structure, deformation potentials, and carrier mobility in strained Si, Ge, and SiGe alloys," *J. Appl. Phys.*, vol. 80, no. 4, pp. 2234–2252, 1996.
- [25] K. Driscoll and R. Paiella, "Silicon-based injection lasers using electronic intersubband transitions in the L valleys," *Appl. Phys. Lett.*, vol. 89, p. 191110, 2006.
- [26] A. Valavanis, " n -Type Silicon-Germanium Based Terahertz Quantum Cascade Lasers," Ph.D. dissertation, University of Leeds, 2009.
- [27] J. Weber and M. I. Alonso, "Near-band-gap photoluminescence of Si-Ge alloys," *Phys. Rev. B*, vol. 40, no. 8, pp. 5683–5693, 1989.
- [28] A. Fropa, P. Handler, F. A. Germano, and D. E. Aspnes, "Electro-absorption effects at the band edges of silicon and germanium," *Phys. Rev.*, vol. 145, no. 2, pp. 575–583, 1966.
- [29] S.-H. Wei and A. Zunger, "Predicted bandgap pressure coefficients of all diamond and zinc-blende semiconductors: Chemical trends," *Phys. Rev. B*, vol. 60, no. 8, pp. 5404–5411, 1999.
- [30] J. Liu, D. D. Cannon, K. Wada, Y. Ishikawa, D. T. Danielson, S. Jongthammanurak, J. Michel, and L. C. Kimerling, "Deformation potential constants of biaxially tensile stressed Ge epitaxial films on Si(100)," *Phys. Rev. B*, vol. 70, no. 15, p. 155309, Oct. 2004.
- [31] L. D. Laude, F. H. Pollak, and M. Cardona, "Effects of uniaxial stress on the indirect exciton spectrum of silicon," *Phys. Rev. B*, vol. 3, no. 8, pp. 2623–2636, Apr. 1971.

- [32] S. L. Chuang, *Physics of Optoelectronic Devices*. New York: Wiley, 1995.
- [33] H. Haug and S. W. Koch, *Quantum Theory of the Optical and Electronic Properties of Semiconductors*. Singapore: World Scientific, 1990.
- [34] B. K. Ridley, *Quantum Processes in Semiconductors*, 4th ed. Oxford, U.K.: Oxford Univ. Press, 1999.
- [35] X. Q. Zhou, H. M. van Driel, and G. Mak, "Femtosecond kinetics of photoexcited carriers in germanium," *Phys. Rev. B*, vol. 50, no. 8, pp. 5226–5230, 1994.
- [36] B. Lax and J. G. Mavroides, "Statistics and galvanomagnetic effects in germanium and silicon with warped energy surfaces," *Phys. Rev.*, vol. 100, no. 6, pp. 1650–1657, 1955.
- [37] A. M. Fox, D. A. B. Miller, G. Livescu, J. E. Cunningham, and W. Y. Jan, "Excitonic effects in coupled quantum wells," *Phys. Rev. B*, vol. 44, no. 12, pp. 6231–6242, Sep. 1991.
- [38] N. Susa, "Improvement in electroabsorption and the effects of parameter variations in the three-step asymmetric coupled quantum well," *J. Appl. Phys.*, vol. 73, no. 2, pp. 932–942, 1993.
- [39] D. Chemla, D. Miller, P. Smith, A. Gossard, and W. Wiegmann, "Room temperature excitonic nonlinear absorption and refraction in GaAs/AlGaAs multiple quantum well structures," *IEEE J. Quantum Electron.*, vol. QE-20, no. 3, pp. 265–275, Mar. 1984.
- [40] C. Lange, N. S. Köster, S. Chatterjee, H. Sigg, D. Christina, G. Isella, H. von Känel, M. Schäfer, M. Kira, and S. W. Koch, "Ultrafast nonlinear optical response of photoexcited Ge-SiGe quantum wells: Evidence for a femtosecond transient population inversion," *Phys. Rev. B*, vol. 79, no. 20, p. 201306, May 2009.
- [41] A. McLean, C. Mitchell, and D. Swanston, "Implementation of an efficient analytical approximation to the voigt function for photoemission lineshape analysis," *J. Electron. Spectr. Related Phenom.*, vol. 69, no. 2, pp. 125–132, 1994.
- [42] L. Lever, Z. Ikončić, A. Valavanis, and R. W. Kelsall, "Design of Ge-SiGe quantum-confined Stark effect modulators for CMOS compatible photonics," *Proc. SPIE*, vol. 7606, 2010.
- [43] Y. Ishikawa, K. Wada, J. Liu, D. D. Cannon, H.-C. Luan, J. Michel, and L. C. Kimerling, "Strain-induced enhancement of near-infrared absorption in Ge epitaxial layers grown on Si substrate," *J. Appl. Phys.*, vol. 98, no. 1, p. 013501, 2005.
- [44] M. Rouviere, M. Halbawax, J.-L. Cercus, E. Cassan, L. Vivien, D. Pascal, M. Heitzmann, J.-M. Hartmann, and S. Laval, "Integration of germanium waveguide photodetectors for intrachip optical interconnects," *Opt. Eng.*, vol. 44, p. 075402, 2005.
- [45] Y. Ishikawa, K. Wada, D. D. Cannon, J. Liu, H.-C. Luan, and L. C. Kimerling, "Strain-induced bandgap shrinkage in Ge grown on Si substrate," *Appl. Phys. Lett.*, vol. 82, no. 13, pp. 2044–2046, 2003.
- [46] J. M. Hartmann, A. Abbadie, A. M. Papon, P. Holliger, G. Rolland, T. Billon, J. M. Fédéli, M. Rouviere, L. Vivien, and S. Laval, "Reduced pressure-chemical vapor deposition of Ge thick layers on Si(001) for 1.3–1.55- μm photodetection," *J. Appl. Phys.*, vol. 95, no. 10, pp. 5905–5913, 2004.
- [47] E. Peiner, A. Gutzzeit, and H.-H. Wehmann, "The effect of threading dislocations on optical absorption and electron scattering in strongly mismatched heteroepitaxial IIIIV compound semiconductors on silicon," *J. Phys.: Condens. Matt.*, vol. 14, no. 48, p. 13195, 2002.
- [48] J. S. H. Yu-Hsuan Kuo, "Thin Buffer Layer for SiGe Growth on Mismatched Substrates," US Patent 077 734, 2007.
- [49] C. Lam, *Passive Optical Networks Principles and Practice*. New York: Elsevier, 2007.
- [50] D. J. Paul, "Si/SiGe heterostructures: From material and physics to devices and circuits," *Semicond. Sci. Technol.*, vol. 19, p. R75R108, 2004.
- [51] J. E. Roth, O. Fidaner, E. H. Edwards, R. K. Schaevitz, Y.-H. Kuo, N. C. Helman, T. I. Kamins, J. S. Harris, and D. A. B. Miller, "C-band side-entry Ge quantum-well electroabsorption modulator on SOI operating at 1 V swing," *Electron. Lett.*, vol. 44, no. 1, Jan. 2008.
- [52] Y.-H. Kuo, Y. K. Lee, Y. Ge, S. Ren, J. E. Roth, T. I. Kamins, D. A. B. Miller, and J. S. Harris, "Quantum-confined stark effect in Ge-SiGe quantum wells on Si for optical modulators," *IEEE J. Sel. Topics Quantum Electron.*, vol. 12, pp. 1503–1513, 2006.
- [53] R. Braunstein, A. R. Moore, and F. Herman, "Intrinsic optical absorption in germanium-silicon alloys," *Phys. Rev.*, vol. 109, no. 3, pp. 695–710, 1958.
- [54] W. L. Bloss, "Linewidths of quantum well eigenstates with finite barriers," *Superlattices Microstruct.*, vol. 7, no. 1, pp. 63–67, 1990.
- [55] D. Y. K. Ko and J. C. Inkson, "Matrix method for tunneling in heterostructures: Resonant tunneling in multilayer systems," *Phys. Rev. B*, vol. 38, no. 14, pp. 9945–9951, Nov. 1988.
- [56] D. J. Dunstan, "Strain and strain relaxation in semiconductors," *J. Materi. Sci.: Mater. Electron.*, vol. 8, pp. 337–375, 1997.
- [57] M. E. Brenchley, M. Hopkinson, A. Kelly, P. Kidd, and D. J. Dunstan, "Coherency strain as an athermal strengthening mechanism," *Phys. Rev. Lett.*, vol. 78, no. 20, pp. 3912–3914, May 1997.
- [58] Comsol Multiphysics, [Online]. Available: www.comsol.com
- [59] M. A. Ordal, R. J. Bell, R. W. Alexander, L. L. Long, and M. R. Querry, "Optical properties of fourteen metals in the infrared and far infrared: Al, Co, Cu, Au, Fe, Pb, Mo, Ni, Pd, Pt, Ag, Ti, V, and W.," *Appl. Opt.*, vol. 24, p. 4493, 1985.
- [60] M. E. Chin and W. S. C. Chang, "Theoretical design optimization of multiple-quantum-well electroabsorption waveguide modulators," *IEEE J. Quantum Electron.*, vol. 29, pp. 2476–2488, 1993.

Leon Lever received the M.Sci. (hons.) degree in physics from the University of Nottingham, U.K., in 2001, and the Ph.D. degree in electronic and electrical engineering from the University of Leeds, U.K., in 2006.

From 2001 to 2002 he worked in the research and development division of Celestion International Limited, and has been with the Institute of Microwaves and Photonics at the University of Leeds, U.K., since 2006. His research interests include intersubband transitions in quantum well devices, quantum cascade lasers, silicon photonics, and SiGe optoelectronic devices.

Zoran Ikončić was born in Belgrade, Yugoslavia, in 1956. He received the B.Sc., M.Sc., and Ph.D. degrees in electrical engineering from the University of Belgrade, in 1980, 1984, and 1987, respectively.

During 1981–1999, he was with the Faculty of Electrical Engineering, University of Belgrade, where he was a Full Professor from 1998. Since 1999, he has been with the School of Electronic and Electrical Engineering, University of Leeds, Leeds, U.K. His current research interests include electronic structure, optical and transport properties of semiconductor nanostructures, and devices based upon them.

Alex Valavanis was born in Maidstone, U.K., in 1981. He received the M.Eng. (hons.) degree in electronic engineering from the University of York, U.K., in 2004, and the Ph.D. degree in electronic and electrical engineering from the University of Leeds, U.K., in 2009.

From 2004 to 2005, he was with the instrumentation division of CCLRC Daresbury Laboratories, Warrington, U.K. He is currently with the Institute of Microwaves and Photonics at the University of Leeds. His research interests include quantum cascade lasers, silicon photonics, terahertz imaging and computational methods for quantum electronics.

Dr. Valavanis is a member of the Institution of Engineering and Technology (IET).

Jonathan D. Cooper was born in Aldershot, U.K., in 1988. He received the B.Eng. (hons.) degree in electronic engineering from the University of Leeds, U.K., in 2009.

Since 2009 he has been studying towards a Ph.D. degree in electronic engineering within the Institute of Microwaves and Photonics at the University of Leeds. His research interests include quantum electronics, computational physics and optoelectronic devices.

Robert W. Kelsall received the B.Sc. (hons.) and Ph.D. degrees in applied physics and electronics from the University of Durham, U.K., in 1985 and 1989, respectively. His doctoral research involved the development of Monte Carlo simulations of electronic transport in GaAs quantum wells.

In 1993, he joined the University of Leeds, U.K., and currently holds the post of Reader in Semiconductor Nanotechnology within the Institute of Microwaves and Photonics at the University of Leeds. His research interests include advanced technology microwave, optoelectronic and molecular electronic devices.

Dr. Kelsall is a Fellow of the U.K. Institute of Physics.